OPEN ACCESS
IOP Publishing | ISECAEP
Journal of Reliability Science and Engineering
J. Reliab. Sci. Eng. 1 (2025) 015006 (16pp)
https://doi.org/10.1088/3050-2454/adbaf6

Design for solar floor tiles systems under competing risks: a case study

Jingzhe Lei[1], **Min Xie**[1] and **Way Kuo**[1,2,*]

[1] Department of Systems Engineering, City University of Hong Kong, Hong Kong Special Administrative Region of China, People's Republic of China
[2] Hong Kong Institute for Advanced Study, City University of Hong Kong, Hong Kong Special Administrative Region of China, People's Republic of China

E-mail: way@cityu.edu.hk

Received 25 November 2024, revised 19 February 2025
Accepted for publication 27 February 2025
Published 17 March 2025

Abstract

Solar pavement has emerged as an innovative form of building-integrated photovoltaics. Reliability analysis and reliability-based optimal design for solar pavement are infrequent. This research represents the pioneering investigation into the optimal reconfiguration design for solar pavements, considering the interchangeability of solar floor tiles amidst competing risks. A Genetic Algorithm with Munkres Assignment Tuning is proposed to initially determine the Pareto optimality of the reconfiguration design and subsequently enhance the systems reliability through minor adjustments. A comprehensive case study for solar floor tiles with total-cross-tied topology is presented to showcase the main idea.

Keywords: solar pavement, reliability-based optimal design, optimal reconfiguration design, solar floor tiles, competing risks, Munkres assignment

1. Introduction

In recent years, advancements in solar technology have led to the development of innovative applications such as building integrated photovoltaics that incorporate solar panels directly into building structures. Pavement-integrated photovoltaic module, or photovoltaic pavement represents an emerging technology that seamlessly incorporates solar panels into the surface of roadways or walkways (Ma *et al* 2019, Hu *et al* 2021). The panel components of the solar pavement system are called solar floor tiles.

Solar floor tiles are installed on sidewalks, cycling paths or even car roads (Mukherjee *et al* 2024). These tiles are specially designed to withstand foot traffic and the weight of vehicles while incorporating solar PV technology. They can convert sunlight into electricity, which can be used to power lighting, signage, electric vehicle charging stations or other low-power devices in the vicinity. Besides, the solar tiles also serve the purpose of facilitating lane heating during winter to prevent hazardous road conditions caused by snow or ice. A brief review of solar pavements is presented in section 2.

The interconnections among the solar floor modules resemble those commonly found in conventional roof-based solar panels. These interconnections include series, parallel, series-parallel (SP), total-cross-tied (TCT), honeycomb (HC), and bridge link (BL) configurations. Numerous researchers have dedicated their efforts to the solar panel reconfiguration design in terms of the aforementioned electric circuit topology structure so as to maximize the power output during operation.

To the best of the authors' knowledge, the existing literature on solar array reconfiguration mostly aims to maximize power generation under partial shading conditions. Narayanaswamy *et al* (2023) categorized the solar array reconfiguration into two distinct types: static reconfiguration (Singh *et al* 2024) and dynamic reconfiguration (Fang and Yang 2024, Sun *et al* 2024, Swetha and Reddy 2024). Static reconfiguration entails

* Author to whom any correspondence should be addressed.

making physical rearrangements, while dynamic reconfiguration involves altering the electrical connections via control switches while retaining the original location of the solar modules. This work pertains to the static reconfiguration type.

The solution techniques for solar topology reconfiguration revolve around heuristic-based, puzzle-based, and machine-learning-based approaches and try to effectively achieve a uniform dispersion of shadow across the solar panel. The following three paragraphs correspond to the three kinds of approaches respectively.

Udenze *et al* (2018) implemented an iterative sorting approach to arrange PV modules in a hierarchical pattern so as to mitigate the impact of mismatch caused by non-uniform aging among PV modules.

Opting for a logic-based number placement puzzle proves to be a favorable approach for generating candidate configurations of solar array matrices (Horoufiany and Ghandehari 2018, Krishna and Moger 2019). Take the most popular puzzle SuDoKu as an example, its objective is to fill a 9×9 grids with digits so that each column, each row, and each of the nine 3×3 subgrids contains all the digits from 1 to 9 without repetition. SuDoKu rules can be appropriately relaxed or strengthened according to the specific scale and configuration settings of the solar array. The universality of SuDoKu make it widely used by scholars. Ahluwalia *et al* (2024) proposed a novel optimized SoDoKu approach to reduce the line losses and mitigate the partial shading effects simultaneously. Other puzzle-based approaches include TomTom puzzle (Tatabhatla *et al* 2020), Ken-ken puzzle (Palpandian *et al* 2021), calcudoku puzzle (Aljafari *et al* 2023), etc.

With the advancement of artificial intelligence, machine learning-based optimization approaches are increasingly gaining popularity and recognition. Deshkar *et al* (2015) presented a genetic algorithm (GA)-based approach for TCT-connected modules in a PV array. Rajan *et al* (2017) adopted standard deviation GA instead. Tatabhatla *et al* (2021) proposed an image processing inspired chaos map reconfiguration. They considered the pixels in an image as panels in a solar array, utilizing this analogy to address the issue of partial shading. Kamal *et al* (2022) introduced artificial neural networks into the solar array reconfiguration. Gao *et al* (2023) demonstrated an unsupervised adaptive technique using Divide and Conquer Q-Learning. Narayanaswamy *et al* (2023) introduced a topology reconfiguration algorithm utilizing deep neural networks (DNNs) regularized with dropout and batch norm, aiming to select the most suitable topology (SP, HC, BL, or TCT) to maximize the power output for a given irradiance profile. Fang and Yang (2024) developed the multiple switching matrices alongside a reconfiguration algorithm with YALMIP optimization toolbox and Gurobi interface for minimizing mismatch loss issue of TCT-based PV arrays. Sun *et al* (2024) introduced a novel adaptive threshold iteration algorithm designed for irradiance equalization in laser wireless power transmission systems. Their approach leveraged DNNs to enhance both the maximum power output and conversion efficiency. Swetha and Reddy (2024) put forth a dual-objective methodology employing the spotted hyena optimization integrated with a non-linear convergence factor (SHO-NCF) for the optimal reconfiguration of PV array subject to partial shading effects.

However, the aforementioned solar array reconfiguration works are quite limited. One limitation of previous studies is their sole focus on the electrical relationships between the panels, with the objective of maximizing power output. Actually, the optimization problem can be very meaningful and insightful from the perspective of reliability engineering, i.e. trying to maximize the reliability or prolong the life of the solar array of interest (Niu *et al* 2021, Kuo *et al* 2022, Prajapati *et al* 2022, Yadav *et al* 2022). While advancements in solar cell technology (such as perovskite solar cells) can achieve high power conversion efficiency, the lifespan of these cells currently spans from mere hours to months (Graniero *et al* 2023), falling short of the industry standard longevity of 25–30 years. As such, reliability-based optimal design plays a vital role for solar systems.

The other limitation is that most of the works only consider the partial shading conditions. Solar floor tiles operate differently from conventional solar modules due to the considerable influence of moving loads, including humans, bicycles, and vehicles, on the panels. Furthermore, it is essential to recognize that there exists a reciprocal relationship between the internal degradation of solar modules and their resilience to external shocks. The performance and reliability of solar pavements are thus affected by competing risks including both the external factors and the internal degradation of the modules.

In order to overcome the aforementioned limitations, our study emphasizes the reliability-based optimal reconfiguration design of solar pavement systems in the presence of competing risks.

To the best of the authors' knowledge, this study marks the first attempt to perform reconfiguration design for the solar floor tiles system. It is also the pioneering work to adopt a reliability engineering perspective, rather than focusing solely on maximizing energy generation, for optimal reconfiguration design. The contributions are outlined below:

- Introduce the innovative solar floor tiles system and its potential in the field of solar energy.
- Develop a reliability assessment model for the solar floor tiles system with TCT topology under competing risks;
- Propose a Genetic Algorithm with Munkres Assignment Tuning to search for the optimal reconfiguration design for solar floor tiles system.

The remainder of this paper is structured as follows: In section 2, a brief literature review on solar pavements is presented. Section 3 outlines the problem statement, including reliability evaluation, the risk factor, the mathematical formulation and the optimization problem of the solar floor tiles systems under consideration. Section 4 provides a detailed explanation of the proposed algorithm, Genetic Algorithm with Munkres Assignment Tuning. A case study is discussed in section 5, and section 6 concludes the paper.

Table 1. Existing solar pavements around the world.

Year	Description	Scale	Location
2013	1st walkable solar pavement	9.29 m^2 27 pavers	George Washington University, USA
2014	1st solar parking lot	40.13 m^2	Sandpoint, Idaho, USA
2014	1st solar bicycle lane	70 m 236.25 m^2	Krommenie, Netherlands
2016	1st solar road 'Wattway'	1000 m 2800 m^2	Tulufur, Normandy
2017	1st solar motorway in China	1080 m 5875 m^2	Jinan, Shandong, China
2017	Solar walkway	80 m^2	Astana, Kazakhstan
2018	1st solar sidewalk paving system at a logistic park	4.7 m^2	Budapest, Hungary
2018	1st solar bicycle lane in Germany	90 m 200 m^2	Erftstadt, Germany
2022	Solar paving	24 pavers	Stellenbosch University, South Africa
2023	Solar paver system at the pedestrian pathway	44 pavers	Hin Keng Station, Hong Kong
2023	Solar floor tiles at HKICE	16 pavers 10.08 m^2	CityU, Hong Kong

2. Review on solar pavements

In this section, we provide a brief introduction on solar pavements and present the existing applications of solar pavements worldwide.

Several research have paved the theoretical fundamentals for the solar pavements. Relevant literatures include: Ma *et al* (2019), Hu *et al* (2021), Li *et al* (2021), Zhou *et al* (2021a), Zhou *et al* (2021b), Li *et al* (2022), Ma *et al* (2022), Hu *et al* (2023), Li *et al* (2023), Zhang *et al* (2023).

In addition to the theoretical advancements in solar pavements, practical applications have emerged worldwide. Table 1 encompasses essential information regarding the construction year, type, scale, and location of the current solar pavements. The type of pavements includes solar walkway, solar bicycle lane, solar motorway, and solar parking lots. The scale (square/length/number of pavers) of the solar pavements is given based on the relevant reports, or estimation given the number and size of the floor tiles.

Using the data from this table, we have created a global solar pavement map, as shown in figure 1, where countries or regions with solar pavements are visually represented by colored areas. The respective scale (in square meters) for countries or regions with solar pavements is illustrated in figure 2. It is evident that this promising technology has not gained widespread popularity globally, particularly in regions (such as the equator) rich in solar energy that is currently being wasted. Additionally, the coverage area of solar floor tiles is severely restricted, typically spanning tens of square meters. Solar pavement at Hong Kong Institute for Clean Energy (HKICE) at City University of Hong Kong is presented in figure 3.

3. Problem statement

The main objective of our study is to adopt a reliability engineering perspective to evaluate and enhance the performance of solar floor tiles systems in the presence of competing risks. To establish this framework, we begin by discussing the fundamental connection topology and reliability evaluation methods in sections 3.1 and 3.2, respectively. Subsequently, we introduce the risk factor associated with solar array configurations. In section 3.4, we formulate the mathematical model for the solar floor tiles system. Section 3.5 constructs the optimization problem.

3.1. Solar PV array configurations

Conventional solar PV array interconnections encompass series, parallel, SP, TCT, BL, and HC connections. The SP topology (figure 4(a)) involves connecting the solar panel strings in parallel, with each string consisting of multiple solar panels connected in series. By combining the series and parallel connections, the SP configuration offers improved energy output, reduced wiring costs, and enhanced performance under partial shading scenarios. The TCT topology (figure 4(b)) is an extension of the SP configuration where cross ties are introduced at the intersections of rows and columns within the SP prototype. It has undergone experimental validation, demonstrating its ability to substantially decrease mismatch losses and enhance the overall output power (Tatabhatla *et al* 2020). BL and HC connections are all variants of SP type and will not be discussed in this work.

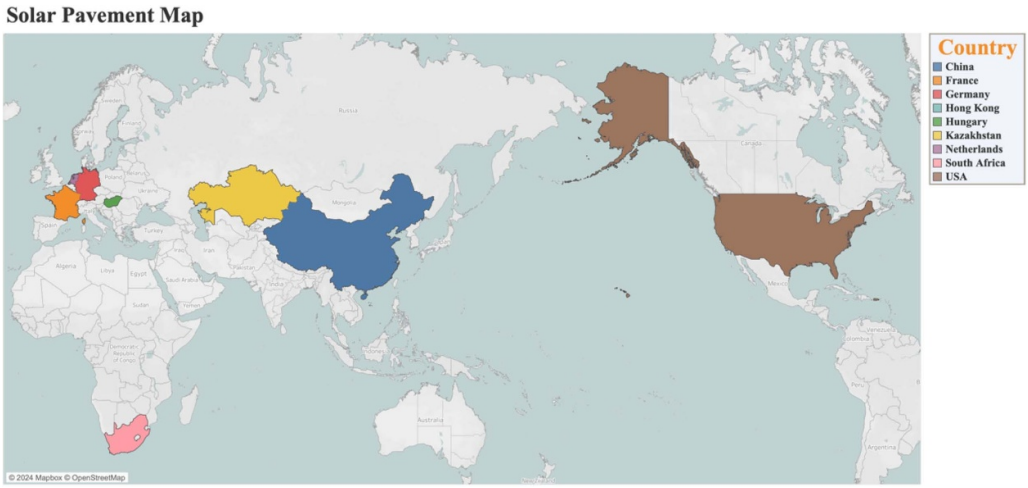

Figure 1. Solar pavement map worldwide.

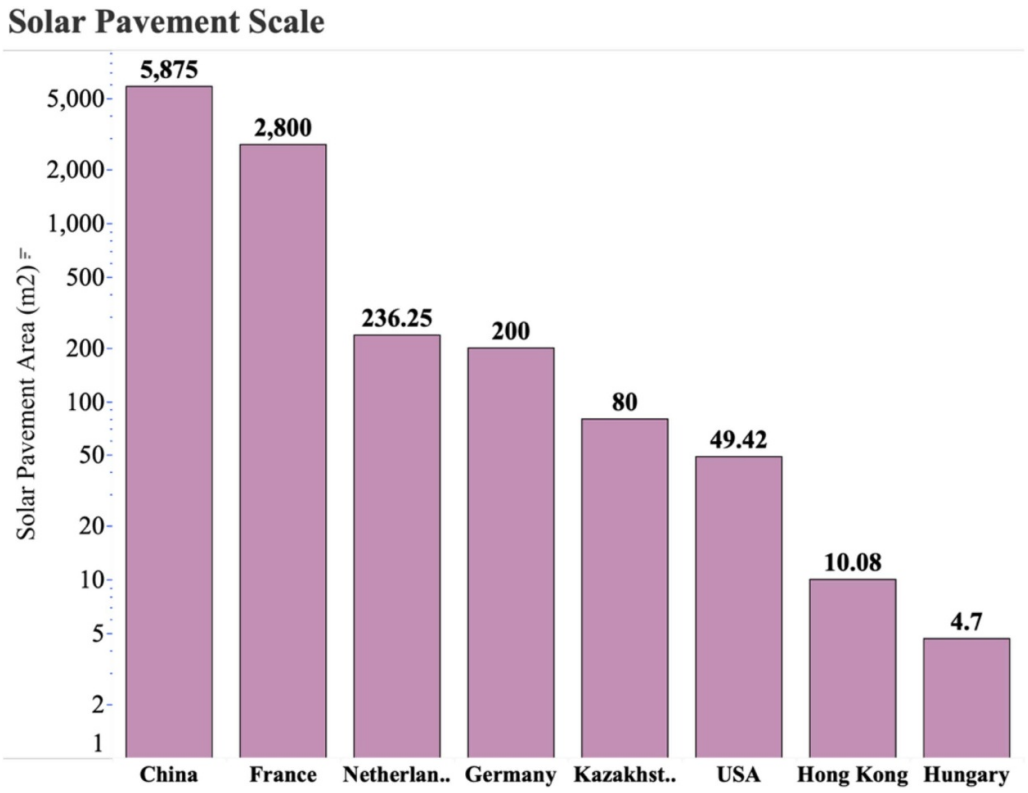

Figure 2. Solar pavement scale worldwide.

The aforementioned topological structures are built upon electromagnetics and involve calculations of voltage, current and final power output. These configurations bear a resemblance to the reliability block diagram commonly employed in the field of reliability engineering. Nevertheless, there is a lack of academic focus on the examination of reliability and the development of reliability-based optimization design, particularly concerning solar PV arrays.

It is important to acknowledge that there exists a distinction in the definitions of configurations between two fields. In fact, even within the field of reliability engineering, there are variations in the nomenclature of the system structures. We adopt the definition provided by Kuo (2001). The topology depicted in figure 4(a) is referred to as the 'parallel-series' structure, while the topology shown in figure 4(b) is referred to as the 'SP' structure.

3.2. *Reliability evaluation*

For a TCT array of size $m \times n$, i.e. m rows and n columns, the time-dependent reliability of the solar array system is expressed as (Gautam and Kaushika 2002):

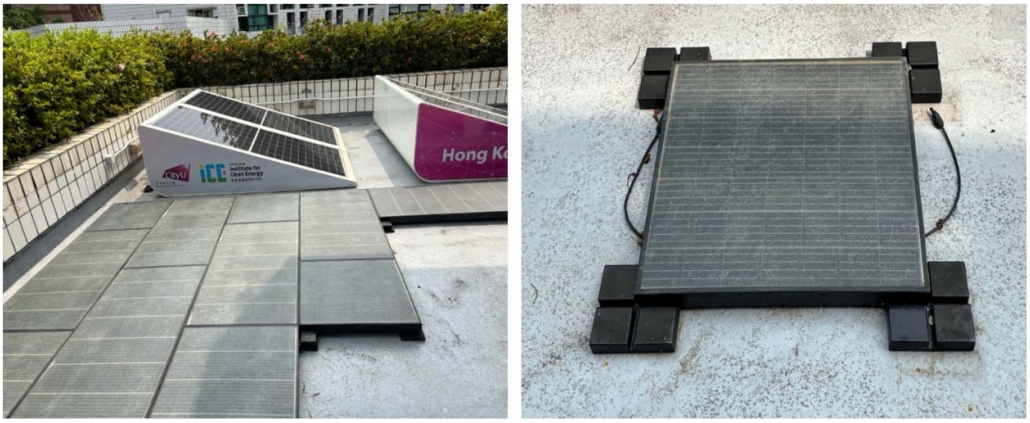

Figure 3. Solar pavement at Hong Kong Institute for Clean Energy (HKICE) at City University of Hong Kong.

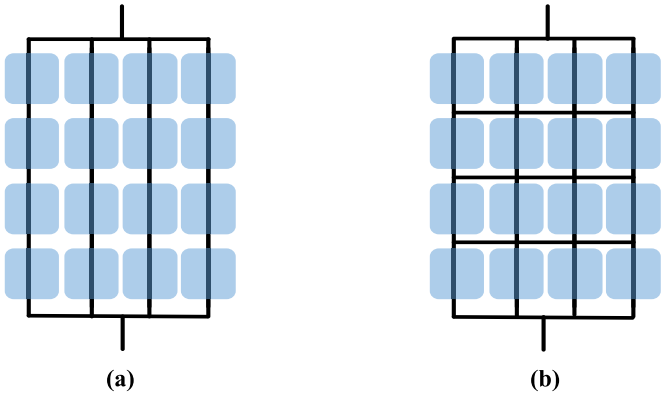

Figure 4. Two common configurations for solar PV array. (*Electronic Engineering Field:* (a) *S*eries-*P*arallel (SP) (b) *T*otal-*C*ross-*T*ied (TCT); *Reliability Engineering Field:* (a) *P*arallel-*S*eries (b) *S*eries-*P*arallel).

$$R_{\mathrm{s}}(t)=\prod_{i=1}^{m}\left(1-\prod_{j=1}^{n}\left(1-r_{ij}(t)\right)\right), \tag{1}$$

where $R_{\mathrm{s}}(t)$ denotes the systems reliability at time t and $r_{ij}(t)$ is the reliability for the solar array at row i column j. Equation (1) is exactly the same as the reliability equation of the SP structure in reliability engineering.

The above reliability expression serves as our optimization objective in this work. The solar panel reliability $r_{ij}(t)$ is measured by the ratio of the power output to the initial output and can be obtained by sensors directly in the real field. For example, the term T_{80} represents the time that the solar cell degrades by 20% of its original performance. In this context, we would determine the solar cell's reliability as 0.8 at T_{80}. For simplicity, we use simulated reliability data in our case study.

It is worth noting that for real-world scenarios where the reliability data for each panel is difficult to obtain or estimate, an alternative structural-based reliability evaluation method can be employed. This approach, which utilizes the sequential failure times of solar modules, offers a viable substitute. Yang *et al* (2024) derived the system reliability through a unique structural reliability treatment, offering a more efficient and accurate reliability evaluation result. Additionally, the order statistics-based system reliability evaluation method proposed by Lei and Kuo (2024) provides another valuable reference for reliability evaluation. Although this condition is not explored further in this paper, it presents a promising direction for future research.

3.3. Competing risks

Both intrinsic and extrinsic factors can induce solar panel degradation. Intrinsic factors are usually related to the materials and manufacturing technology, including discoloration, browning, and delamination of the ethylene vinyl acetate copolymer. While extrinsic factors are primarily environmental factors such as solar radiation, humidity, wind, extreme temperatures, dust, etc. It is worth noting that these risk factors can interact and mutually influence the degradation process of solar panels.

The failures of the solar floor tiles can be classified as soft and hard failures. A soft failure is jointly determined by the internal continuous degradation and abrupt degradation increments, or degradation rate increments induced by the stress of external shock arrivals. A hard failure occurs when the external shocks or impacts directly render the component or system inoperable. The shocks on the components/systems can trigger system failure or degradation. The occurrence of soft failures can also increase the vulnerability of components/system to hard failures. Specifically, shocks can cause damage or wear to the solar panels, leading to eventual panel failure and decreased reliability. Also, a panel that is already weakened by a soft failure is more susceptible to damage from an external shock.

In our framework, we incorporate a risk factor w, which varies between 0 and 1, indicating the level of risk associated with each panel. The set of panel risk factors constitutes a risk matrix W given the solar array dimension. Each element $w_{ij} \in [0,1]$ in W represents the normalized risk intensity for panel at row i, column j, where $w_{ij} \to 1$ indicates high-risk exposure. Two approaches can be used for determining W in real scenarios:

1. Expert knowledge: for systems lacking sensor data, domain expertise guides risk assignments.
2. Sensor-driven evaluation: sensor-based tracking—such as pressure detectors measuring mechanical stresses (e.g. from high heels or heavy loads) and light sensors quantifying shading duration or coverage area—also informs the risk matrix W.

Take the solar floor tile system with two equivalently dominant external risks (high-heel pressure $w_{ij}^{(1)}$ and pedestrian flow-induced shading $w_{ij}^{(2)}$) as an example. Pressure sensors quantify $w_{ij}^{(1)}$ for the module at row i, column j; light sensors translate shading duration/area into $w_{ij}^{(2)}$. The composite risk factor $w_{ij} = 0.5\, w_{ij}^{(1)} + 0.5\, w_{ij}^{(2)}$. This 50–50 weighting reflects equal prioritization of pressure and shading effects, and the risk weighting coefficients are modifiable to align with different operating environments.

3.4. Mathematical model

As mentioned in the introduction, solar roads can extend over significant distances, often spanning hundreds of meters. For instance, the solar road in Tourouvre-au-Perche stretches across a distance of 1 km, and the Dutch government plans to construct a solar bicycle lane that covers 500 m. When considering such extensive installations, it becomes evident that relocating a solar floor tile to a distant location poses significant challenges, including the necessity for specialized equipment, the inherent risks of potential damage, and the substantial investment of time and resources. Consequently, opting for such a relocation solution is unviable and economically inefficient, necessitating the need to divide the solar floor tile system into manageable blocks to ensure practicality and cost-effectiveness.

Each block allows for the interchangeability of solar modules within its boundaries, while modules from distinct blocks cannot be exchanged. The coverage area of each block can be determined based on expert knowledge or physical limitations, such as the presence of zebra lines or other factors.

Assume the solar floor block is of regular rectangle pattern with m rows and n columns. Then the tile index at the very beginning stage (i.e. before reconfiguration) can be expressed in matrix form $\mathbf{\Pi}^0 = (\pi_{i,j})_{m\times n}$. The matrix form is more straightforward for understanding but not convenient enough for the optimization procedure. Hence, we introduce the corresponding vector form by stacking the columns of $\mathbf{\Pi}^0$ and adjusting the subscript from 1 to $(m \times n)$ as outlined below:

$$\begin{aligned}\mathbf{\Pi}^0 &= [\pi_{1,1}, \pi_{2,1}, \ldots, \pi_{m,1}, \pi_{1,2}, \pi_{2,2}, \ldots, \pi_{m,2}, \ldots, \\ &\quad \pi_{1,n}, \pi_{2,n}, \ldots, \pi_{m,n}] \\ &= [\pi_1, \pi_2, \ldots, \pi_{m\times n}]\,.\end{aligned}$$

Without loss of generality, set $\pi_i = i$ $(i = 1, 2, \ldots, m \times n)$, i.e.

$$\mathbf{\Pi}^0 = [1, 2, \ldots, m \times n]\,.$$

On the basis of the initial solar floor index vector, we introduce the corresponding reliability vector as:

$$\boldsymbol{R}^0 = [r_1, r_2, \ldots, r_{m\times n}]\,.$$

Unless explicitly stated to use matrix form, vector form is used by default. The use of superscripts is employed to distinguish between different stages. $\mathbf{\Pi}^0$ denotes the initial state, $\mathbf{\Pi}^1$ represents the intermediate state and $\mathbf{\Pi}^2$ is the final reconfiguration vector. Similarly, the reliability vector is labeled as $\boldsymbol{R}^0, \boldsymbol{R}^1, \boldsymbol{R}^2$, corresponding to the respective stages. The detailed meaning for different states will be covered in section 4.3.

Now we use a simple example shown in figure 5 to explain how the reconfiguration works. A solar floor tiles system with 2 rows and 3 columns is presented here. Initially, the configuration is set as $\mathbf{\Pi}^0 = [1, 2, 3, 4, 5, 6]$ by default. The corresponding reliability vector is $\boldsymbol{R}^0 = [r_1, r_2, r_3, r_4, r_5, r_6]$. The subscript of the reliability vector is always the same as the element in the same position of configuration vector.

Besides, we also introduce the distance measure D and the systems reliability measure R_s. Euclidean metric is used to assess the moving distance, and the distance between two adjacent row or column is set as unit 1. In practical scenarios where the width and length of the tiles are known, the distance metrics can be adjusted to accurately represent the real physical distances between tile centers.

Systems reliability evaluation for TCT configuration is shown in equation (1). Algorithm 1 demonstrates the details. Our objective for the optimal reconfiguration design is to minimize the moving distance D while maintaining the systems reliability R_s above a predetermined threshold.

3.5. Optimization problem

In the context of the solar floor tiles system, our objective is to enhance the overall performance of the system in a cost-effective manner through the redistribution of tiles. By integrating the two aforementioned metrics, our objective is to minimize the overall displacement distances, while ensuring that the system's reliability remains above a predetermined threshold c_0 (for example, 0.8).

The initial configuration vector is

$$\begin{aligned}\mathbf{\Pi}^0 &= [\pi_{1,1}, \pi_{2,1}, \ldots, \pi_{m,1}, \pi_{1,2}, \pi_{2,2}, \ldots, \pi_{m,2}, \ldots, \\ &\quad \pi_{1,n}, \pi_{2,n}, \ldots, \pi_{m,n}] \\ &= [1, 2, \ldots, m \times n]\,.\end{aligned}$$

Denote the ultimate configuration vector as

$$\begin{aligned}\mathbf{\Pi}^2 &= [\tilde{\pi}_{1,1}, \tilde{\pi}_{2,1}, \ldots, \tilde{\pi}_{m,1}, \tilde{\pi}_{1,2}, \tilde{\pi}_{2,2}, \ldots, \tilde{\pi}_{m,2}, \ldots, \\ &\quad \tilde{\pi}_{1,n}, \tilde{\pi}_{2,n}, \ldots, \tilde{\pi}_{m,n}]\,,\end{aligned}$$

which is a permutation of $[1, 2, \ldots, m \times n]$.

Regarding the distance element d_k $(k = 1, 2, \ldots, m \times n)$ obtained in Step 1 of algorithm 1, it records the movement distance of transferring panel i. Now rearrange the distance

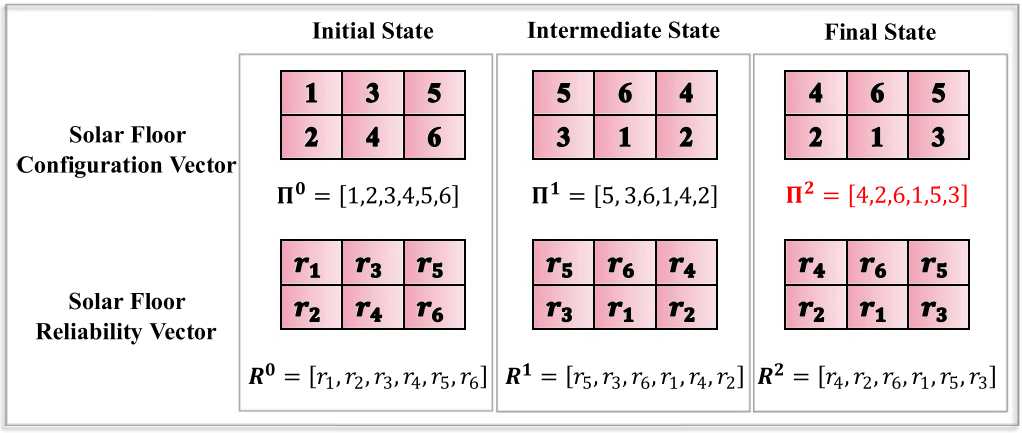

Figure 5. Vector form of a solar floor tiles system with 2 rows and 3 columns.

Algorithm 1. Moving distance and systems reliability assessment.

Input: Two configurations $\boldsymbol{\Pi}_{m\times n}, \tilde{\boldsymbol{\Pi}}_{m\times n}$ in matrix form;
Corresponding reliability vector $\boldsymbol{R}_{m\times n}, \tilde{\boldsymbol{R}}_{m\times n}$ in matrix form.

Output: Total moving distance $D = \mathrm{dis}\left(\boldsymbol{\Pi}, \tilde{\boldsymbol{\Pi}}\right)$;
Systems reliability $R_{\mathrm{s}}(\boldsymbol{\Pi})$, $R_{\mathrm{s}}\left(\tilde{\boldsymbol{\Pi}}\right)$.

1: For $k = 1 : (m \times n)$
Return the row and column index of k in $\boldsymbol{\Pi}$: $r_{\boldsymbol{\Pi}}$, $c_{\boldsymbol{\Pi}}$;
Return the row and column index of k in $\tilde{\boldsymbol{\Pi}}$: $r_{\tilde{\boldsymbol{\Pi}}}$, $c_{\tilde{\boldsymbol{\Pi}}}$;
Calculate the Euclidean distance $d_k = \sqrt{\left(r_{\boldsymbol{\Pi}} - r_{\tilde{\boldsymbol{\Pi}}}\right)^2 + \left(c_{\boldsymbol{\Pi}} - c_{\tilde{\boldsymbol{\Pi}}}\right)^2}$.
End
Sum the distances together: $D = \sum_{k=1}^{m\times n} d_k$.

2: Systems reliability under configuration $\boldsymbol{\Pi}$: $R_{\mathrm{s}}(\boldsymbol{\Pi}) = \prod_{i=1}^{m}\left(1 - \prod_{j=1}^{n}(1 - R_{ij})\right)$
Systems reliability under configuration $\tilde{\boldsymbol{\Pi}}$: $R_{\mathrm{s}}\left(\tilde{\boldsymbol{\Pi}}\right) = \prod_{i=1}^{m}\left(1 - \prod_{j=1}^{n}\left(1 - \tilde{R}_{ij}\right)\right)$.

elements to a distance matrix:

$$(d_{i,j})_{m\times n} = \begin{bmatrix} d_{\tilde{\pi}_{1,1}} & d_{\tilde{\pi}_{1,2}} & \dots & d_{\tilde{\pi}_{1,n}} \\ d_{\tilde{\pi}_{2,1}} & d_{\tilde{\pi}_{2,2}} & \dots & d_{\tilde{\pi}_{2,n}} \\ \vdots & \vdots & \dots & \vdots \\ d_{\tilde{\pi}_{m,1}} & d_{\tilde{\pi}_{m,2}} & \dots & d_{\tilde{\pi}_{m,n}} \end{bmatrix}.$$

Then the optimization problem can be formulated as follows:

$$\min \sum_{i=1}^{m}\sum_{j=1}^{n} d_{\tilde{\pi}_{i,j}} \tag{2.1}$$

$$\text{s.t.}\,\tilde{\pi}_{i,j} \in \{1,\dots,m\times n\}, \forall i = 1,\dots,m; j = 1,\dots,n; \tag{2.2}$$

$$\sum_{i=1}^{m}\sum_{j=1}^{n} I_{\{\tilde{\pi}_{i,j}=k\}} = 1, \forall k = 1,2,\dots,m\times n; \tag{2.3}$$

$$\prod_{i=1}^{m}\left(1 - \prod_{j=1}^{n}\left(1 - \tilde{R}_{ij}\right)\right) > c_0, \tag{2.4}$$

where $d_{\tilde{\pi}_{i,j}}$ represents the cost for relocating the panel originally at row i column j and equation (2.1) is the optimization objective to minimize the overall total moving distance $\mathrm{dis}\left(\boldsymbol{\Pi}^0, \boldsymbol{\Pi}^2\right)$; equations (2.2) and (2.3) impose a constraint that $\boldsymbol{\Pi}^2$ is a permutation of $[1,2,\dots,m\times n]$, with $I_{\{\tilde{\pi}_{i,j}=k\}}$ being the indicator function corresponding to $\tilde{\pi}_{i,j} = k$; the systems reliability requirement to exceed a predefined threshold c_0 is presented in equation (2.4).

4. Methodology

This section provides the methodology for addressing the aforementioned optimal reconfiguration design. Section 4.1 provides a concise overview of the genetic algorithm and

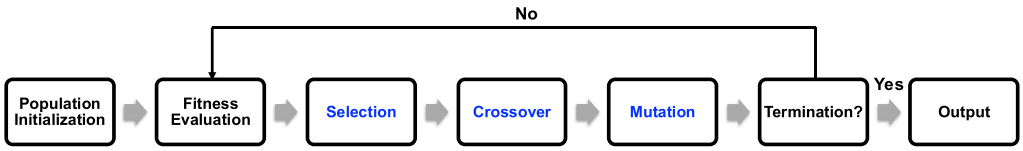

Figure 6. Flowchart of genetic algorithm.

section 4.2 showcases the Munkres Assignment Problem. Our proposed approach, Genetic Algorithm with Munkres Assignment Tuning (GAMA), is thoroughly explained in section 4.3.

4.1. Genetic algorithm

The genetic algorithm is a meta-heuristic randomized search algorithm for optimization, drawing inspiration from natural evolution and Charles Darwin's theory of natural selection. It follows the principle of 'survival of the fittest' to guide the search process. The GA consists of five key stages as shown in figure 6:

(1) **Population initialization**: the initial population consists of a set of individuals, each carrying their own unique set of genes.
(2) **Fitness evaluation**: the fitness function assesses the survival score of each individual;
(3) **Selection**: individuals with higher scores have a greater likelihood of reproduction and gene propagation;
(4) **Crossover**: genes from parent individuals are randomly exchanged with each other, generating offspring with combined traits.
(5) **Mutation**: to introduce diversity and prevent premature convergence, some genes undergo random changes at a low mutation rate.

The above process is repeated until a convergence condition is satisfied or the maximum number of generations is reached. Throughout these iterations, the genetic algorithm explores and refines the solution space, aiming to identify optimal or near-optimal solutions for the given problem. The Genetic Algorithm Toolbox in Matlab provides built-in functions and will be adopted in our study.

4.2. Munkres assignment problem

The assignment problem has been thoroughly investigated within the realm of graph theory in mathematics. Munkres (1957) elucidated the assignment problem and the transportation problem, and he demonstrated a step-by-step approach to solve these optimization problems using Konig's independent zeros theory. Basically, the assignment problem involves the task of selecting the most advantageous assignment of h men to h jobs, considering that numerical ratings are provided for each man's performance on each job. An ideal assignment is one that maximizes the total sum of the men's ratings for the jobs they are assigned to.

In the absence of any shortcuts or optimizations, the enumeration-based strategy requires searching through a feasible region that has a dimension of $h!$. Munkres algorithm has a maximum number of operations $\left(11h^3+12h^2+31h\right)/6$, which is considerably more favorable than the factorial of h. The Munkres assignment (MA) algorithm is also referred to as Kuhn–Munkres (KM) algorithm or Hungarian algorithm (Kuhn 1955). Hungarian algorithm is generally a non-weighted version of KM algorithm.

Since its proposal, Munkres assignment algorithm has found extensive applications in various domains, including PV array reconfiguration (Pachauri *et al* 2022), smart delivery assignment (Vásconez *et al* 2024), UAV swarm takeoff or air traffic management (Hernández *et al* 2021, Lorünser *et al* 2022), weapon target assignment (Truong *et al* 2021), and assignment of reviewers to papers (Kalmukov 2020), etc.

The mathematical formulation of a standard Munkres assignment problem is as follows:

$$\min \sum_{i=1}^{n}\sum_{j=1}^{n} c_{i,j}x_{i,j} \tag{3.1}$$

$$\text{s.t.} \sum_{j=1}^{n} x_{i,j} = 1, \forall i = 1,2,\ldots,n; \tag{3.2}$$

$$\sum_{i=1}^{n} x_{i,j} = 1, \forall j = 1,2,\ldots,n; \tag{3.3}$$

$$x_{i,j} \in \{0,1\}, \forall i,j = 1,2,\ldots,n, \tag{3.4}$$

where $x_{i,j}$ indicates whether assigning the ith personnel to the jth job, and $c_{i,j}$ evaluates the job fitting rate of the ith personnel to the jth job. Equations (3.2)–(3.4) stipulate that there must be a one-to-one mapping between the jobs and personnel.

Unlike the above square matrix setting, the rectangular assignment problem allows for unequal numbers of rows (personnel) and columns (jobs) in the assignment matrix. This means that there can be redundant choices (jobs) or candidates (personnel), making it more general and flexible. Assume the number of personnel is smaller than that of the jobs, i.e. $m < n$, then the problem formulation is as follows:

$$\min \sum_{i=1}^{m}\sum_{j=1}^{n} c_{i,j}x_{i,j} \tag{4.1}$$

$$\text{s.t.,} \sum_{j=1}^{n} x_{i,j} = 1, \forall i = 1,2,\ldots,m; \tag{4.2}$$

$$\sum_{i=1}^{m} x_{i,j} \leqslant 1, \forall j = 1,2,\ldots,n; \tag{4.3}$$

Table 2. The comparison of the two steps in GAMA approach.

	Step 1	Step 2
Approach	Genetic algorithm (GA)	Munkres assignment algorithm (MA)
Objective	Higher systems reliability, Shorter moving distance	Minimize moving distance while maintaining the systems reliability in Step 1
Effect	Row determination	Column determination
Output	Intermediate state: $\mathbf{\Pi}^1$; Pareto front	Final state: $\mathbf{\Pi}^2$

Table 3. Parametric expression and relationship of the distance and reliability measure for the solar floor tiles system.

	Initial State	Intermediate State	Final State
Distance		$D^1 = \mathrm{dis}\left(\mathbf{\Pi}^0, \mathbf{\Pi}^1\right)$	$D^2 = \mathrm{dis}\left(\mathbf{\Pi}^0, \mathbf{\Pi}^2\right)$
Systems Reliability	$R_s^0 = R_s\left(\mathbf{\Pi}^0\right)$	$R_s^1 = R_s\left(\mathbf{\Pi}^1\right)$	$R_s^2 = R_s\left(\mathbf{\Pi}^2\right)$
Relationship		$R_s^0 < R_s^1 = R_s^2; D^1 > D^2$	

$$x_{i,j} \in \{0,1\}, \forall i = 1,2,\ldots,m; j = 1,2,\ldots,n. \tag{4.4}$$

The key distinction arises in equation (4.3), which indicates the possibility of certain jobs not being assigned to any person.

In the upcoming section, we will demonstrate how to leverage the strengths of both the genetic algorithm and the rectangular assignment algorithm (Markus 2024) to explore the optimal reconfiguration strategy for solar floor tile systems.

4.3. Proposed approach: GAMA

In order to evaluate the attainable solutions, we introduced a methodology referred to as Genetic Algorithm with Munkres Assignment Tuning. GAMA can be divided into two steps. The first step facilitates GA to determine which row each floor tile component should be relocated in. And the second step further decides the column index for each solar floor tile with MA algorithm. The reconfiguration strategy obtained in the first step is what we call the intermediate state in figure 5, and the reconfiguration topology after the second step is the final state in figure 5.

The GA is employed to improve the systems reliability, and the MA is utilized to minimize the distance while maintaining the reliability unchanged. Our objective is to identify a reconfiguration strategy that minimizes the distance while ensuring that the system's reliability remains above a pre-defined threshold. In order to ensure that our approach can provide feasible solutions for multiple possible thresholds simultaneously, we introduce a Pareto front that comprises a set of reconfiguration solutions, achieving Pareto optimality in terms of both reliability and distance measures. Pareto optimality, also known as Pareto efficiency, is a concept in economics and game theory that describes a situation where it is impossible to make any one individual better off without making someone else worse off. That is to say, GA cannot find a better reconfiguration topology that achieve higher systems reliability and lower moving distance at the same time. Enhancing one measure would inevitably involve sacrificing the performance of the other variable.

Considering the characteristic of the TCT topology, exchanging the components within a parallel sub-system would not affect the systems reliability, but can make a difference on the moving distance. Therefore, the above reconfiguration strategies can be further improved by the Munkres assignment algorithm. For each row, we apply the MA to obtain the tuned reconfiguration strategy with minimal moving distance.

The comparison of the two steps in GAMA approach is listed in table 2, and table 3 presents the parametric expression and relationship of the distance and reliability measure for the solar floor tiles system. The pseudo algorithm is provided in algorithm 2.

5. Case study

To facilitate the analysis, a simulation approach is adopted using the Weibull distribution combined with the risk factor. In real scenario, the risk factor matrix W can be determined by expert knowledge or evaluated by sensors. Additionally, internal degradation can be gauged by examining the ratio of power output to the initial power output.

The pdf of Weibull distribution is given by

$$f(x;\alpha,\beta) = \frac{\alpha}{\beta}\left(\frac{x}{\beta}\right)^{\alpha-1} \mathrm{e}^{-\left(\frac{x}{\beta}\right)^{\alpha}}, \tag{5}$$

where α is the shape parameter and β is the scale parameter.

The experimental computer is equipped with an 8-core CPU with 6 performance cores and 2 efficiency cores, 16G RAM, and Apple M1 Pro GPU. The modeling is performed using Matlab software.

5.1. 10 × 6 solar floor tiles system

As illustrated in figure 7(a), a reliability matrix $\boldsymbol{R}^0$ is generated by incorporating the degradation mode following the Weibull distribution. A heatmap representation of the reliability matrix $\boldsymbol{R}^0$ is then provided. To facilitate the tracking of the reallocation pattern, the reliability values within each row are sorted

Algorithm 2. Genetic algorithm with Munkres assignment tuning (GAMA).

Input:	Power output ratio matrix $\boldsymbol{P}$ Reliability threshold c_0 ($c_0 = 0.8$ without special demonstration) Weighted risk factor matrix $\boldsymbol{W}$
Output:	Reconfiguration design matrix $\boldsymbol{\Pi}^2$; Systems reliability after reconfiguration R_S^2.
1:	Evaluate reliability measure matrix: $\boldsymbol{R} = \boldsymbol{P}.*\boldsymbol{W}$
2:	Evaluate initial systems reliability Rel $(\boldsymbol{R})$
3:	Obtain mediate reconfiguration design $\boldsymbol{\Pi}^1$ by GA 3.1 Fitfunc1$= R_s(\boldsymbol{\Pi}')$; # Fitness function 1: Systems reliability 3.2 Fitfunc2$=$ dis $(\boldsymbol{\Pi}^0, \boldsymbol{\Pi}')$; # Fitness function 2: Moving distance 3.3 $\boldsymbol{\Pi}' =$ gamultiobj ([Fitfunc1, Fitfunc2]). # Find Pareto optimality 3.4 $\boldsymbol{\Pi}^1 =$ argmin (Fitfun2) s.t. Fitfun1 $> c_0$ # Refine the solutions
4:	Refine the above strategy by MA 4.1 For $i = 1 : m$ $\Pi_i =$ Munkres (D_i) ; # Obtain tuning strategy for each row End 4.2 $\boldsymbol{\Pi}^2 = [\Pi_1; \Pi_2; \ldots; \Pi_m]$.
5:	Evaluate final systems reliability $R_S^2 = R_s(\boldsymbol{\Pi}^2)$.

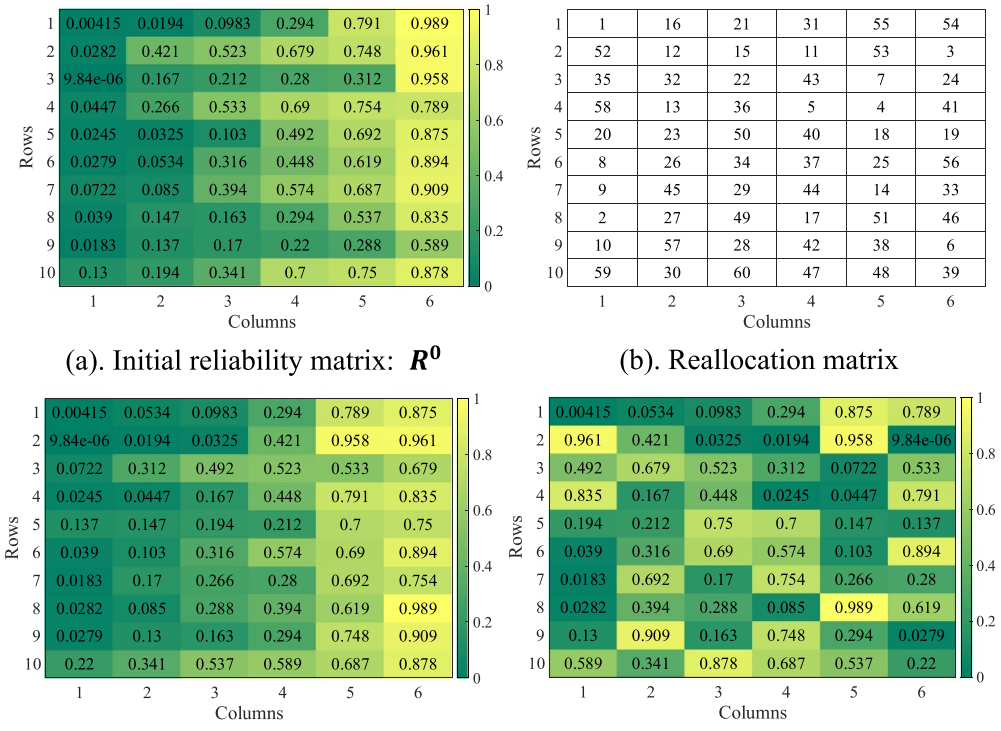

(a). Initial reliability matrix: $\boldsymbol{R^0}$

(b). Reallocation matrix

(c). Final reliability matrix sorted in ascending order

(d). Final reliability matrix: $\boldsymbol{R^2}$

Figure 7. Heatmap of reliability matrix and reallocation 10×6 matrix for solar floor tiles system.

in ascending order. Tiles with reliability close to zero (indicated by dark green) can be considered as failures. The presence of imbalanced reliability among each row can lead to a lower overall systems reliability under TCT configuration.

When assuming the reliability threshold as $c_0 = 0.8$, the final reallocation matrix $\boldsymbol{\Pi}^2$ is given in figure 7(b), wherein each number corresponds to the index of the original tiles. Initially, for the first column, the tiles are indexed from 1 to 10

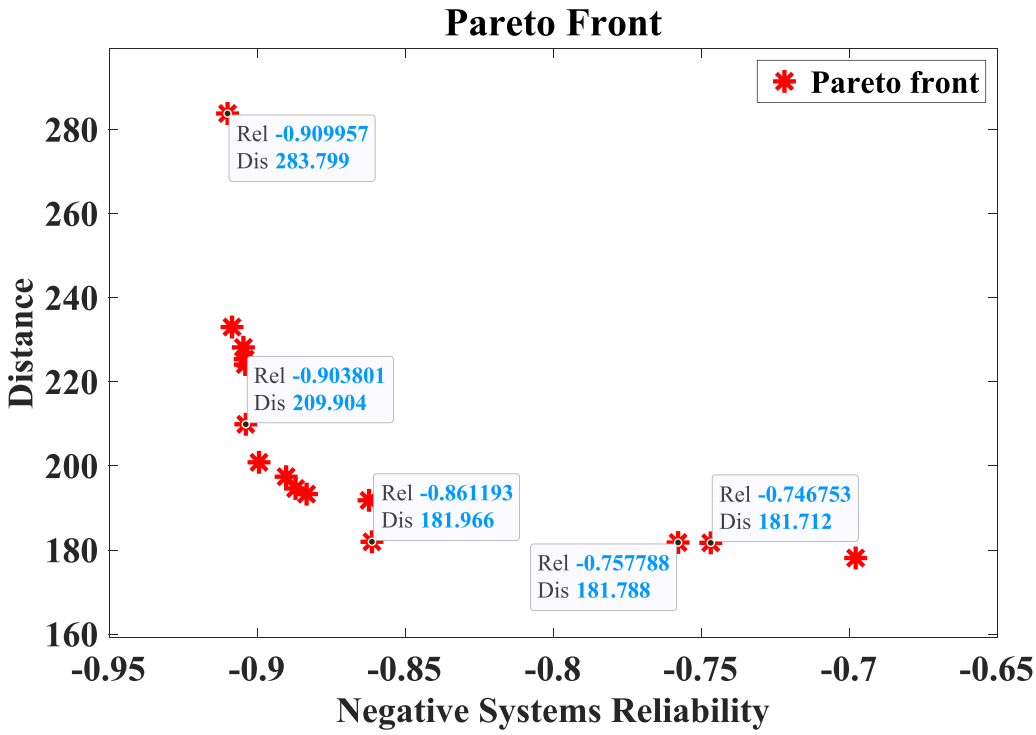

Figure 8. Pareto front of feasible design solutions for 10 × 6 solar floor tiles system (elapsed time is 2929 s.).

from top to bottom, while the second column is indexed from 11 to 20, and so forth. By examining the reallocation matrix $\mathbf{\Pi}^2$, it is suggested to retain tile 1 in its original position and relocate tile 2, previously located in row 2 column 1, to row 8 column 1, and so on. Under the reconfiguration strategy $\mathbf{\Pi}^2$, we can attain a systems reliability of 0.86 while keeping the moving distance at 179.7.

To facilitate the tracking of the configuration pattern, the final reliability matrix $\boldsymbol{R}^2$ is sorted in ascending order for each row. The sorted version is provided in figure 7(c), which is only used for validating the effect of the reconfiguration design. The final reliability matrix $\boldsymbol{R}^2$ is shown in figure 7(d). By comparing figures 7(a) and (c), it becomes evident that the tiles are now balanced across each row.

In figure 8, we present the Pareto front of the feasible solutions obtained by the build-in function '*gamultiobj*' in Matlab in the first step of GAMA. Given our objective of enhancing the reliability and reducing the distance, while the '*gamultiobj*' function aims to minimize both decision variables, we adopt a workaround by representing the reliability variable as negative values in the optimization process.

When $c_0 = 0.8$, the solution suggested by Pareto front can attain a systems reliability of 0.86 and moving distance of 181.97. This demonstrates that Munkres assignment algorithm can reduce the distance measure from 181.97 to 179.7 while keeping the systems reliability at 0.86. MA partially addresses the limitations of GA concerning population size settings and other computational constraints.

As mentioned above, Pareto front can deal with the scenario when a set of possible thresholds are taken into account simultaneously. Consider a series of reliability thresholds $[0.7, 0.75, 0.8, 0.85, 0.9]$. We label the ideal solutions in table 4 according to figure 8. $c_0 = 0.8$ and $c_0 = 0.85$ share the same design in our case. We give the reconfiguration design matrix $\mathbf{\Pi}^2$ for $c_0 = 0.9$ in figure 9 compared to the design for $c_0 = 0.8$ in figure 7(b).

Table 4. Performance of designs obtained by Pareto front for different thresholds.

Reliability threshold	Systems reliability	Distance
0.7	0.7468	181.71
0.75	0.7578	181.79
0.8	0.8612	181.97
0.85	0.8612	181.97
0.9	0.9038	209.90

It should be pointed out that the Pareto front obtained in Step 1 of GAMA not only serves as a guide for our optimization problem outlined in equations (2.1)–(2.4) but also provides reference solutions for the single-objective optimization problem to maximize the systems reliability while disregarding the moving distance. The optimal solution at this time is located at the upper-left characterized by a reliability of 0.91 and a corresponding distance of 283.8.

5.2. 15 × 15 solar floor tiles system

This subsection delves into a larger-scale scenario involving a 15 × 15 solar floor tiles system. The initial reliability matrix $\boldsymbol{R}^0$ is depicted in figure 10(a). Without loss of generality, each

Rows \ Columns	1	2	3	4	5	6
1	1	29	46	18	21	53
2	54	22	11	28	58	5
3	4	13	31	34	36	55
4	7	50	42	17	26	59
5	3	14	24	35	60	56
6	51	15	9	16	43	2
7	27	32	33	37	47	48
8	45	57	10	12	49	23
9	8	20	19	25	38	52
10	44	40	6	39	41	30

Figure 9. Reallocation matrix $\mathbf{\Pi}^2$ when $c_0 = 0.9$.

row is sorted in ascending order by the reliability value, facilitating the examination of the distribution pattern of reliability levels.

The Pareto front displaying feasible design solutions is illustrated in figure 11. Opting for a threshold of 0.82 on this occasion, we will select the solution that attains a final reliability of 0.8203, accompanied by a moving distance of 1545.13.

The reallocation matrix $\mathbf{\Pi}^2$ is displayed in figure 10(b). For illustration, consider the solar floor tile initially situated at index 1 with a reliability of 0.00207; it has since been repositioned to row 2, column 8. Figures 10(c) and (d) depict the final dispersion mode of reliability and the final reliability matrix $\boldsymbol{R}^{\mathbf{2}}$, respectively.

In the high-dimensional scenario, the TCT configuration notably enhances system robustness, leading to a high overall system reliability. Consequently, the impact of reconfiguration on improvement is less pronounced compared to the 10×6 case.

5.3. 100×4 solar floor tiles system

We now examine a 100×4 solar floor tiles system, which is well-suited for a solar roadway. The reliability matrix and reallocation matrix are too large to visualize directly. Instead, we only compare the dispersion pattern of reliability matrix before and after reconfiguration design.

Given that the most reliable solar panels in each row have substantial influence on the system's overall reliability under the TCT configuration, our heatmap predominantly highlights the dispersion of a subset of elements exhibiting relatively higher reliability. Ideally, post-sorting each row based on reliability values, these high-reliability components should locate predominantly in column 4.

Figure 12 shows that the reliability matrix initially has a considerable portion in column 3, but after reconfiguration, there is a notable shift where the high-reliability components become more concentrated in column 4. This outcome confirms the efficacy of the reconfiguration design and showcases the applicability of GAMA to high-dimensional cases.

5.4. Comparative analysis

This subsection is devoted to provide the comparative optimization results of our proposed GAMA to other traditional meta-heuristic optimization algorithms, including 1. Genetic algorithm (GA); 2. Particle swarm optimization (PSO); 3. Simulated annealing (SA); 4. Multi-objective genetic algorithm (MOGA).

Two main challenges for our optimization problem are:

(1) **Objective**: our optimization problem involves a bi-objective optimization of systems reliability and moving distance of solar floor tiles system;
(2) **Design variable**: our optimization problem requires finding an optimal choice for a high-dimensional integer vector that must be a permutation of 1 to n, where n is the number of solar floor tiles in the system of interest.

Single-objective optimization is applied to GA, PSO, and SA to identify the reconfiguration strategy that achieves the highest reliability. In contrast, bi-objective optimization is conducted using MOGA and GAMA to explore feasible Pareto solutions that balance higher reliability with reduced moving distance. The dimension setting is the same as section 5.1, that is, we use a 10×6 solar floor tiles system as an example. The comparison results are shown in table 5.

From table 5, it can be observed that while GA, PSO, and SA are capable of achieving solutions with high system reliability, they result in relatively high moving distances, which can lead to increased economic costs. MOGA, on the other hand, provides a set of feasible solutions based on a predefined reliability threshold. Our proposed GAMA further reduces the distance metric while maintaining the same level of reliability obtained by MOGA. The strengths and limitations of the various optimization algorithms can be summarized as follows:

1. GA, PSO, and SA generally yield a single solution. In contrast, MOGA and GAMA generate a Pareto front, providing a spectrum of feasible solutions that enable decision-makers to select strategies flexibly according to specific practical scenarios.
2. GAMA, which is an enhancement of MOGA, incorporates the Munkres Algorithm. This refinement preserves the reliability achieved by MOGA while further minimizing the moving distance.

5.5. Discussion on scalability

We have examined three dimensional configurations for the reconfiguration design: 10×6, 15×15, 100×4. Next, we will discuss the scalability of our proposed method from the following two aspects.

1. **Dimension limitation**: ultra-large dimensions are excluded in our research considering the maintenance feasibility (as relocating to remote regions could incur high labor costs) and electrical losses. To strike a balance

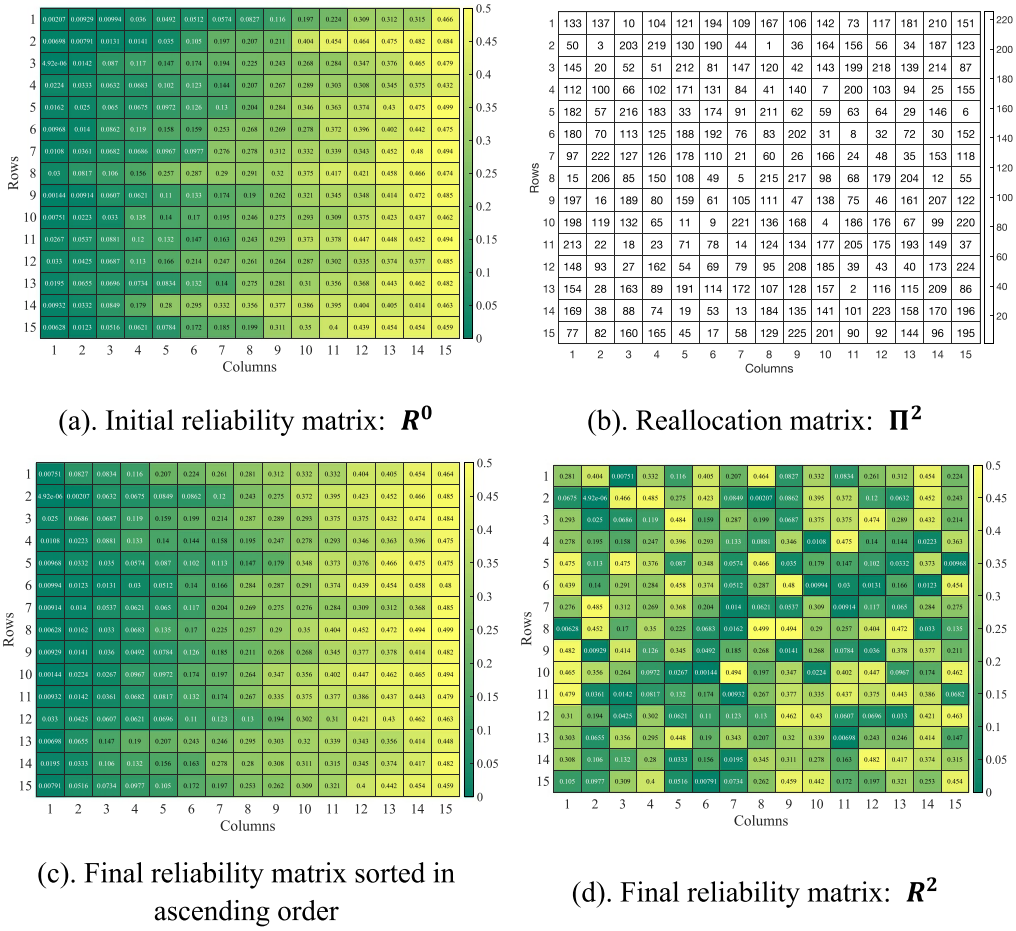

(a). Initial reliability matrix: $\boldsymbol{R^0}$

(b). Reallocation matrix: $\boldsymbol{\Pi^2}$

(c). Final reliability matrix sorted in ascending order

(d). Final reliability matrix: $\boldsymbol{R^2}$

Figure 10. Heatmap of reliability matrix and reallocation matrix for 15 × 15 solar floor tiles system.

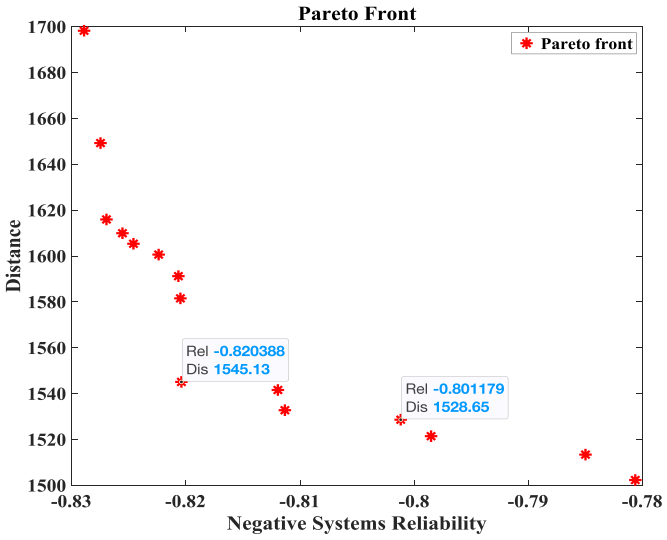

Figure 11. Pareto front of feasible design solutions for 15 × 15 solar floor tiles system (elapsed time is 8460 s.).

between scalability and practicality, we limited our testing to dimensions up to 100 × 4. For larger deployments, solar arrays can be partitioned into sub-blocks optimized independently via the GAMA framework.

2. **Parameter configuration**: the runtime is highly dependent on the hyperparameter selection. In our case studies, we intentionally selected large population sizes in GA to ensure precise reliability assessments for safety-critical systems. That is why the experiment time for generating Pareto fronts may extend to hours. For less critical scenarios like residential installations, the parameters can be relaxed and feasible solutions meeting reliability thresholds can be achieved within seconds or minutes.

In summary, the GAMA framework can adequatedly address real-world scenarios within reasonable timeframes under current computational paradigms. However, methods that achieve higher efficiency, such as GPU acceleration, remain desirable and represent a promising direction for future research.

6. Conclusions

This work focuses on the reconfiguration design of the solar floor tiles system under competing risks. Notably, this research is the first to undertake an optimal design of solar arrays from the perspective of reliability engineering. Two decision variables are considered. One is the system's reliability, the other is the moving distance when transferring

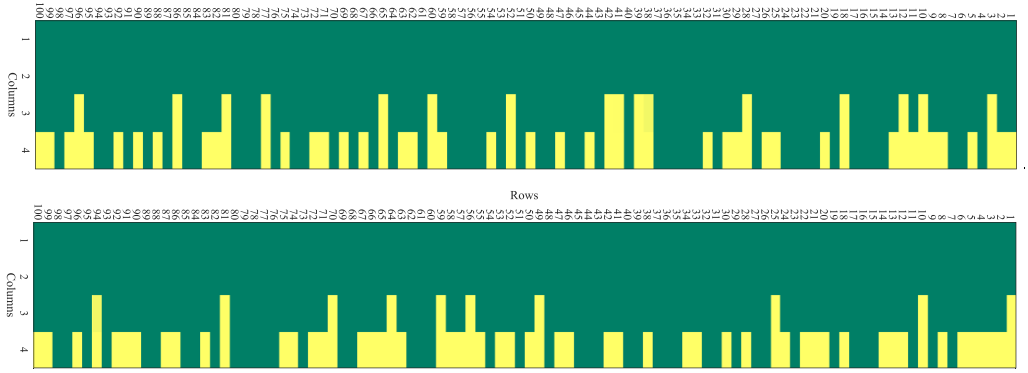

Figure 12. Heatmap of reliability matrix for 100 × 4 solar floor tiles system (top: reliability dispersion before reconfiguration; bottom: reliability dispersion after reconfiguration).

Table 5. Performance comparison of different optimization algorithms.

Algorithms	Final reliability	Moving distance	Reconfiguration matrix	Reliability threshold
GA	0.9040	225.71	2 36 35 17 40 54 1 56 6 31 42 7 45 5 25 28 14 53 4 12 50 33 46 47 18 41 15 21 34 44 30 10 9 8 43 51 48 20 60 24 19 39 59 55 27 26 22 49 57 38 37 16 32 13 29 3 11 52 58 23	
PSO	0.9045	248.36	17 2 12 48 52 8 18 6 57 34 9 49 31 42 47 36 46 28 39 10 13 19 14 53 7 22 11 4 30 51 24 38 43 54 41 16 29 45 32 56 3 35 1 60 55 26 23 15 33 59 50 27 5 44 20 58 25 37 40 21	
SA	0.9137	241.56	39 44 34 45 33 31 26 14 56 28 42 18 8 9 4 11 51 19 10 6 17 13 47 53 55 25 15 41 16 46 49 60 23 29 37 32 40 3 30 54 21 50 59 7 58 48 27 36 20 2 22 43 52 1 35 12 24 57 38 5	
MOGA	0.7468	181.71		$c = 0.7$
	0.7578	181.79		$c = 0.75$
	0.8612	181.97		$c = 0.8, 0.85$
	0.9038	209.90		$c = 0.9$
GAMA	**0.8612**	**179.70**	Shown in figure 9.	$c = 0.8, 0.85$

the floor tiles. Our objective is to minimize the moving distance while ensuring the systems reliability exceeds a predetermined threshold or a set of thresholds. Genetic Algorithm with Munkres Tuning approach is proposed for solving the optimal design problem. A case study of a solar floor tiles systems with 10 rows, 6 columns and 5 possible reliability thresholds is provided to showcase our idea. This is followed by two larger-scale experiments conducted with dimensions of 15 × 15 and 100 × 4. A comparative analysis with other meta-heuristic optimization algorithms is also included to highlight the advantages of the proposed GAMA method.

As a pioneering study in the field of reconfiguration design for solar pavement systems, there are several aspects that warrant further exploration and can serve as future research directions. To begin with, it is important to consider the presence of diverse floor tile types within a single system, which can vary in terms of size, load capacity, stress requirements, and other factors, thereby introducing the challenge of tackling the multi-type assembly problem. Second, due to constraints imposed by the physical environment, real-world scenarios often involve irregular patterns instead of the rectangular shape in our work. Moreover, employing advanced algorithmic strategies (such as parallel computing

architectures and GPU-accelerated optimization) to fine-tune the GAMA approach can improve the computation efficiency in high-dimensional scenarios. Last but not least, importance measure (Kuo and Zhu 2012) can be combined into the framework to guide the optimization design.

Acknowledgment

The authors would like to thank the Hong Kong Institute for Clean Energy (HKICE) for the kind support of case study.

Conflict of interest

The authors have no conflicts of interest to declare that are relevant to the content of this article.

ORCID iD

Jingzhe Lei https://orcid.org/0000-0003-2222-3742

References

Ahluwalia D, Anjum S and Mukherjee V 2024 Comprehensive analysis of line losses and valuation of energy savings in optimized photovoltaic array subjected to partial shadings *Energy Convers. Manage.* **301** 118034

Aljafari B, Devakirubakaran S, Bharatiraja C, Balachandran P K and Babu T S 2023 Power enhanced solar PV array configuration based on calcudoku puzzle pattern for partial shaded PV system *Heliyon* **9** e16041

Buehren M 2024 Functions for the rectangular assignment problem *MATLAB Central File Exchange* (available at: www.mathworks.com/matlabcentral/fileexchange/6543-functions-for-the-rectangular-assignment-problem) (Accessed 9 May 2024)

Deshkar S N, Dhale S B, Mukherjee J S, Babu T S and Rajasekar N 2015 Solar PV array reconfiguration under partial shading conditions for maximum power extraction using genetic algorithm *Renew. Sustain. Energy Rev.* **43** 102–10

Fang X and Yang Q 2024 Dynamic reconfiguration of photovoltaic array for minimizing mismatch loss *Renew. Sustain. Energy Rev.* **191** 114160

Gao X, Deng F, Wu G, Pan Q, Zheng C, Wang W, Cai T and Jiang L 2023 Divide and Conquer Q-Learning (DCQL) algorithm based photovoltaic (PV) array reconfiguration scheme for alleviating the partial shading influence *Sol. Energy* **249** 21–39

Gautam N K and Kaushika N D 2002 Reliability evaluation of solar photovoltaic arrays *Sol. Energy* **72** 129–41

Graniero P, Khenkin M, Köbler H, Hartono N T P, Schlatmann R, Abate A, Unger E, Jacobsson T J and Ulbrich C 2023 The challenge of studying perovskite solar cells' stability with machine learning *Front. Energy Res.* **11** 1118654

Hernández D, Cecília J M, Calafate C T, Cano J C and Manzoni P 2021 The Kuhn-Munkres algorithm for efficient vertical takeoff of UAV swarms *2021 IEEE 93rd Vehicular Technology Conf. (Vtc2021-spring)* (IEEE) pp 1–5

Horoufiany M and Ghandehari R 2018 Optimization of the Sudoku based reconfiguration technique for PV arrays power enhancement under mutual shading conditions *Sol. Energy* **159** 1037–46

Hu H, Vizzari D, Zha X and Mantalovas K 2023 A comparison of solar and conventional pavements via life cycle assessment *Transp. Res.* D **119** 103750

Hu H, Vizzari D, Zha X and Roberts R 2021 Solar pavements: a critical review *Renew. Sustain. Energy Rev.* **152** 111712

Kalmukov Y 2020 An algorithm for automatic assignment of reviewers to papers *Scientometrics* **124** 1811–50

Kamal S, Ramapraba P S, Kumar A, Saha B C, Lakshminarayana M, Sanal Kumar S, Gopalan A and Erko K G 2022 Optimization of solar panel deployment using machine learning *Int. J. Photoenergy* **2022** 7249109

Krishna S G and Moger T 2019 Optimal SuDoKu reconfiguration technique for total-cross-tied PV array to increase power output under non-uniform irradiance *IEEE Trans. Energy Convers.* **34** 1973–84

Kuhn H W 1955 The Hungarian method for the assignment problem *Nav. Res. Logist. Q.* **2** 83–97

Kuo T C, Pham T T, Huang P T, Nguyen H T, Bui D M and Le P D 2022 Reliability analysis of PV generating systems in the islanded DC microgrid under dynamic and transient operation *IET Renew. Power Gener.* **16** 988–1026

Kuo W 2001 *Optimal Reliability Design: Fundamentals and Applications* (Cambridge University Press)

Kuo W and Zhu X 2012 Some recent advances on importance measures in reliability *IEEE Trans. Reliab.* **61** 344–60

Lei J and Kuo W 2024 An order statistics perspective for system reliability *Appl. Stoch. Models Bus. Ind.* (https://doi.org/10.1002/asmb.2895)

Li S, Chen Z, Liu X, Zhang X, Zhou Y, Gu W and Ma T 2021 Numerical simulation of a novel pavement integrated photovoltaic thermal (PIPVT) module *Appl. Energy* **283** 116287

Li S, Gu W, Liu X, Zhou Y, Chen Z, Zhang X and Ma T 2022 Pavement integrated photovoltaic thermal (PIPVT) system: a temporal and spatial analysis of energy and exergy performance *J. Clean. Prod.* **340** 130782

Li S, Ma T and Wang D 2023 Photovoltaic pavement and solar road: a review and perspectives *Sustain. Energy Technol. Assess.* **55** 102933

Lorünser T, Wohner F and Krenn S 2022 A verifiable multiparty computation solver for the linear assignment problem: and applications to air traffic management *Proc. 2022 on Cloud Computing Security Workshop* pp 41–51

Ma T, Li S, Gu W, Weng S, Peng J and Xiao G 2022 Solar energy harvesting pavements on the road: comparative study and performance assessment *Sustain. Cities Soc.* **81** 103868

Ma T, Yang H, Gu W, Li Z and Yan S 2019 Development of walkable photovoltaic floor tiles used for pavement *Energy Convers. Manage.* **183** 764–71

Mukherjee A, Benett J, Anyigor K T, Olayinka O B O, Khalafallah A M, Alencastro J and Butt T E 2024 Solar roads–a new potential renewable energy for and Great Britain *Environ. Technol.* **45** 5956–65

Munkres J 1957 Algorithms for the assignment and transportation problems *J. Soc. Ind. Appl. Math.* **5** 32–38

Narayanaswamy V, Ayyanar R, Tepedelenlioglu C, Srinivasan D and Spanias A 2023 Optimizing solar power using array topology reconfiguration with regularized deep neural networks *IEEE Access* **11** 7461–70

Niu M, Xu N Z, Kong X, Ngin H T, Ge Y Y, Liu J S and Liu Y T 2021 Reliability importance of renewable energy sources to overall generating systems *IEEE Access* **9** 20450–9

Pachauri R K, Minai A F, Kuchhal P and Jha V 2022 Munkres assignment algorithm for optimal reconfiguration to improve GMPP of partially shaded PV array system *2022 4th Int. Conf. on Circuits, Control, Communication and Computing (I4C)* (IEEE) pp 193–8

Palpandian M, Winston D P, Kumar B P, Kumar C S, Babu T S and Alhelou H H 2021 A new ken-ken puzzle pattern based reconfiguration technique for maximum power extraction in partial shaded solar PV array *IEEE Access* **9** 65824–37

Prajapati S, Soni Y P and Fernandez E 2022 Energy harvesting with photovoltaic arrays: assessment of reliability with alternative configurations for power delivery *Smart Structures in Energy Infrastructure: Proc. ICRTE 2021* vol 2 (Springer) pp 167–73

Rajan N A, Shrikant K D, Dhanalakshmi B and Rajasekar N 2017 Solar PV array reconfiguration using the concept of standard deviation and genetic algorithm *Energy Proc.* **117** 1062–9

Singh R, Yadav V K and Singh M 2024 Performance enhancement of a novel reduced cross-tied PV arrangement under irradiance mismatch scenarios *Appl. Energy* **376** 124185

Sun Y, Deng G, Yang H, Chen Y, Gou Y and Wang J 2024 Dynamic reconfiguration of photovoltaic arrays for laser wireless power transmission via deep neural networks *IEEE Trans. Power Electron.* **39** 7708–20

Swetha K T and Reddy B V 2024 An effective dual-objective optimization to enhance power generation in a two-stage grid-tied PV system under partial shading conditions *Energy* **305** 132259

Tatabhatla V M R, Agarwal A and Kanumuri T 2020 Minimising the power loss of solar photo voltaic array through efficient reconfiguration of panels *Proc. Inst. Mech. Eng.* A **234** 690–708

Tatabhatla V M R, Agarwal A and Kanumuri T 2021 A chaos map based reconfiguration of solar array to mitigate the effects of partial shading *IEEE Trans. Energy Convers.* **37** 811–23

Truong N X, Phuong P K and Tien V H 2021 Fast and simple method for weapon target assignment in air defense command and control system *Int. Conf. on Industrial Networks and Intelligent Systems* (Springer) pp 403–15

Udenze P, Hu Y, Wen H, Ye X and Ni K 2018 A reconfiguration method for extracting maximum power from non-uniform aging solar panels *Energies* **11** 2743

Vásconez J P, Schotborgh E, Vásconez I N, Moya V, Pilco A, Menéndez O, Guamán-Rivera R and Guevara L, 2024. Smart delivery assignment problem through machine learning and the Munkres algorithm (https://doi.org/10.20944/preprints202403.1703.v1)

Yadav G, Joshi D, Gopinath L and Soni M K 2022 Reliability and availability optimization of smart microgrid using specific configuration of renewable resources and considering subcomponent faults *Energies* **15** 5994

Yang L, Zhang X, Lu Z, Fu Y, Moens D and Beer M 2024 Reliability evaluation of a multi-state system with dependent components and imprecise parameters: a structural reliability treatment *Reliab. Eng. Syst. Saf.* **250** 110240

Zhang Y, Ma T, Yang H, Li Z and Wang Y 2023 Simulation and experimental study on the energy performance of a pre-fabricated photovoltaic pavement *Appl. Energy* **342** 121122

Zhou B, Pei J, Calautit J K, Zhang J and Guo F 2021a Solar self-powered wireless charging pavement—a review on photovoltaic pavement and wireless charging for electric vehicles *Sustain. Energy Fuels* **5** 5139–59

Zhou B, Pei J, Nasir D M and Zhang J 2021b A review on solar pavement and photovoltaic/thermal (PV/T) system *Transp. Res.* D **93** 102753

Jingzhe Lei received the B.S. degree in mathematics and applied mathematics from University of Science and Technology of China, Hefei, China, in 2021. She is currently working toward the PhD degree in industrial engineering with the Department of Systems Engineering, City University of Hong Kong, Hong Kong. Her current research interests include optimal reliability design and order statistics-based reliability analysis.

Min Xie is currently the Chair Professor with the Department of Systems Engineering, City University of Hong Kong, Hong Kong. He authored or coauthored more than 300 peer reviewed journal articles and 8 books on quality and reliability engineering. More than 50 PhD students have graduated under his supervision.

Prof. Xie was elected as a member of the European Academy of Science and Arts in 2022. He is an Editor and an Associate Editor and on the editorial board of many established international journals. He has chaired many international conferences and given keynote speeches. He was a recipient of the Prestigious Lee Kuan Yew Research Fellowship in 1991.

Way Kuo is a Senior Fellow of Hong Kong Institute for Advanced Study. He served as President and University Distinguished Professor of City University of Hong Kong between 2008 to 2023. A pioneer in reliability research of systems at their infant stage, Professor Kuo is renowned for his work in designing the reliability of electronics and energy systems. He is a Member of US National Academy of Engineering and Academia Sinica in Taiwan, a Foreign Member of Chinese Academy of Engineering and an International Fellow of Canadian Academy of Engineering.